Nanoscale

Accepted Manuscript

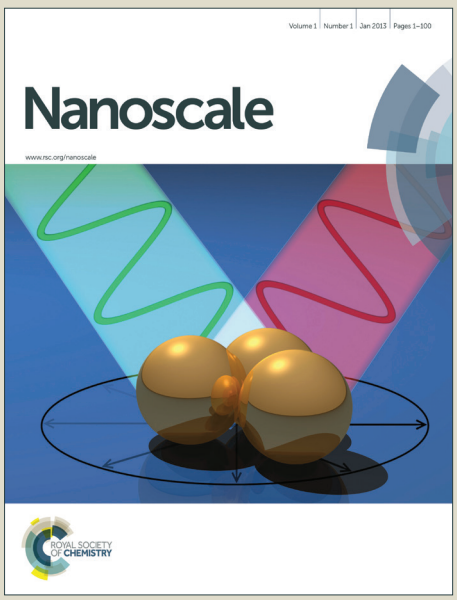

ROYAL SOCIETY OF CHEMISTRY

www.rsc.org/nanoscale

Nanoscale

RSCPublishing

ARTICLE

Fabrication of white electroluminescent device based on bilayered yellow and blue quantum dots

Cite this: DOI: 10.1039/xoxxoooooox

Jong-Hoon Kim,[a] Ki-Heon Lee,[a] Hee-Don Kang,[a] Byoungnam Park,[a] Jun Yeon Hwang,[b] Ho Seong Jang,[c] Young Rag Do[d] and Heesun Yang*[a]

Received ooth January 2012,
Accepted ooth January 2012

DOI: 10.1039/xoxxoooooox

www.rsc.org/

Till now most work on colloidal quantum dot-light-emitting diode (QLED) has been focused on the improvement of electroluminescent (EL) performance of monochromatic device, and multi-colored white QLED comprising more than one type of QD emitter has been rarely investigated. To demonstrate a white EL as a result of color mixing between blue and yellow, herein, a unique combination of two dissimilar QDs of blue- CdZnS/ZnS plus yellow-emitting Cu–In–S (CIS)/ZnS is used for the formation of emitting layer (EML) of multilayered QLED. First, the QLED consisting of a single EML randomly mixed with two QDs is fabricated, however, its EL is dominated by a blue emission with the contribution of yellow one substantially weak. Thus, another EML configuration is devised in the form of QD bilayer with two stacking sequences of CdZnS/ZnS // CIS/ZnS QD and *vice versa*. The QLED with the former stacking sequence shows an overwhelming contribution of blue EL, similar to the mixed QD EML-based device. Upon applying the oppositely stacked QD bilayer of CIS/ZnS // CdZnS/ZnS, however, a bicolored white EL can be successfully achieved by means of the effective extension of radiative excitonic recombination zone throughout both QD EML regions. Such QD EML configuration-dependent EL results, which are discussed primarily by the proposed device energy level diagram, strongly suggest that the positional designing of individual QD emitters is a critical factor for the realization of multicolored, white emissive devices.

1 Introduction

Thanks to the beneficial fluorescent attributes including high photoluminescent (PL) efficiency and facile emission wavelength tunability, semiconductor quantum dots (QDs) have rapidly emerged as alterative visible emitters to conventional inorganic bulk phosphors and organic luminophores. Thus, QDs have been regarded as active optical materials for the fabrication of light-emitting devices, specifically by replacing inorganic phosphors of color-converted light-emitting diodes (LEDs) and small molecules/polymers of organic LEDs (OLEDs). Color-conversion QD-LEDs are rather technologically mature and thus right in front of commercialization. On the other hand, electrically-driven or electroluminescent (EL) QLEDs still remain in the early stage of development, even though the substantial improvements in device performance have been achieved for recent years. A remarkable QLED performance was realized through multilayered structure with a hybrid combination of organic hole transport layer (HTL) plus inorganic electron transport layer (ETL). ZnO, in particular, in the form of nanoparticles (NPs), is most commonly chosen as an inorganic ETL primarily due to its high electron mobility as well as favorable energetic alignment with the conduction band level of QDs.[1-7] In 2011, Holloway and coworkers reported peak values of current efficiency (CE) of 7.5 cd/A and external quantum efficiency (EQE) of 1.8% from green (540 nm) QLED.[1] Later, Mashford's group demonstrated even higher EL characteristics such as a peak CE of 19 cd/A and an EQE of ~18% (*i.e.*, an internal quantum efficiency of near 90%) from an inverted-structured red (~612 nm) QLED.[4] Most recently, the record EQE of 20.5%, corresponding to a theoretical maximum, was accomplished by Peng *et al.* from red (640 nm) QLED, where 6 nm-thick insulating layer of poly(methyl methacrylate) (PMMA) was inserted between QD emitting layer (EML) and ZnO ETL in order to limit current density across the device and thus optimize charge balance.[5] All QLEDs aforementioned commonly comprised II–VI QDs, where the presence of Cd is indispensable for securing visible spectral range.

Non-Cd QDs with the typical compositions of III–VI (*e.g.*, InP) and I–III–VI groups (*e.g.*, Cu–In–S (CIS), Zn–Cu–In–S (ZCIS), Cu–In–Ga–S) can be also applied as active emissive layers of QLEDs. In the early phase of investigation on both III–VI and I–III–VI QLEDs, their device structure consisted of the QD EML sandwiched with organic HTL and ETL.[8-12] Subsequently, analogous to II–VI QLEDs, organic ETL has been replaced with inorganic ZnO NPs, leading to similarly beneficial effects on device performance. For instance, upon applying ZnO NP ETL green InP QLED reached a peak EQE of 3.46%,[13] whose value is markedly high compared to that (*i.e.*, <0.01%) from the earlier organic ETL-based counterpart.[8] Such an efficacy of ZnO NP ETL can be also found in I–III–VI QLEDs. While peak CEs of organic ETL-integrated CIS and ZCIS QLEDs ranged within 0.62–0.92 cd/A,[11,12] at least fourfold CE increase of 4.15 cd/A was obtainable from ZnO NP ETL-based CIS device.[14]

As described above, most effort on QLED fabrication has been dedicated to EL performance improvement of monochromatic device. However, from a standpoint of practical application of QLEDs to general illumination and display, multicolored white EL should be

pursued. Kim *et al.* demonstrated the fabrication of a full-color white QLED as a display device, where red, green, and blue II–VI QD EMLs were sequentially patterned by a solvent-free transfer printing.[15] A more convenient approach for the realization of white EL is to form the EML mixed with multicolored QDs. The fabrication of white QLED, comprising a mixed red, green, and blue II–VI QD monolayer along with two neighboring organic HTL and ETL, was implemented, exhibiting peak EL values of 0.9 cd/A (CE), 0.36% (EQE), and 830 cd/m^2 (luminance).[16] Very recently, adopting the same approach of mixed II–VI QD EML (1–2 monolayer) as above, Bae *et al.* reported better-performance trichromatic (red, green, blue) and tetrachromatic (red, yellow, cyan, blue) white QLEDs integrated with ZnO NP ETL. The resulting QLEDs showed peak EQEs of 0.9–1.3% and peak luminances of 5340–6400 cd/m^2, depending on the type of device.[17]

Bicolored white emission through typically color-mixing blue and yellow has been the most common type in color conversion LEDs for general lighting. In such lighting-targeted white device a broad spectral coverage is preferred to secure a high color rendering index (CRI). In this context, nod-Cd I–III–VI QDs may be promising yellow emitters, since they provide an intrinsically broad emission bandwidth as a result of radiative recombination *via* intra-gap defect states.[18-21] To realize a bicolored white EL device a blue QD emitter is needed, however, non-Cd blue QDs are not practically available from I–III–VI and III–V compositions. In the case of I–III–VI QDs, their substantial Stokes shift of emission *versus* absorption due to the above defect-related recombination renders the acquisition of blue emission almost implausible. Meanwhile, synthesis of blue InP QDs appear feasible, however, their size must be extremely tiny for a strong quantum confinement effect and thus their PL efficiency is expected to be low inappropriately for device application, attributable to the presence of high density of surface state and/or the difficulty of complete shelling of such small-sized InP core.[22] To develop a bicolored white lighting EL device, herein, a unique combination of two core/shell QDs of blue II–VI CdZnS/ZnS and yellow I–III–VI CIS/ZnS is chosen for EML formation of multilayered hybrid QLED having an HTL of poly(9-vinlycarbazole) (PVK) and an ETL of ZnO NPs. Firstly, similar to the above literature,[16,17] the QLED with a single EML of randomly-mixed CdZnS/ZnS and CIS/ZnS QD, is fabricated, but its EL is governed dominantly by blue emission with yellow emission substantially quenched. Then, the formation of bilayered QD EML is devised with two configurations of opposite stacking sequence, *i.e.*, CdZnS/ZnS // CIS/ZnS and *vice versa*. While an overwhelming blue EL from CdZnS/ZnS // CIS/ZnS QD bilayer is observed, the QLED with the other sequence of CIS/ZnS // CdZnS/ZnS QD bilayer successfully exhibits a bicolored white EL. The sensitiveness of EL behaviors to the EML configuration is highlighted and detailed EL performance of white QLEDs is reported.

2 Experimental

2.1 Synthesis of CdZnS/ZnS, CIS/ZnS QDs and ZnO NPs

Blue-emitting CdZnS/ZnS QDs were prepared following the synthetic protocol reported previously by our group[6,23] with a slight modification, specifically changing the amount of sulfur in core synthesis in order to tune the emission wavelength. Yellow CIS/ZnS QDs were also synthesized based on our recipe published earlier.[14,24] As-synthesized QDs were repeatedly purified and re-dispersed in hexane with appropriate concentrations for EML formation. ZnO NPs with a size range of 3.0–3.5 nm were synthesized using a solution-precipitation process reported in literature,[1] and dispersed in ethanol for ETL formation. The synthetic details of the above QDs and NPs were described in Supporting Information.

2.2 Fabrication of Multilayered QLEDs

A patterned indium tin oxide (ITO) (a sheet resistance of ~20 Ω sq^{-1}) glass substrate was cleaned sequentially with DI water, acetone, and methanol, and then UV-ozone treated for 20 min. ~25 nm-thick poly(ethylenedioxythiophene):polystyrene sulphonate (PEDOT:PSS, AI 4083) as a hole injection layer (HIL) was spin-deposited (3000 rpm, 60 s), and baked at 150^{o}C for 30 min in N_2 atmosphere. On top of HIL, using a solution of 0.05 g PVK (average M_W = 25000–50000) dissolved in 5 ml of chlorobenzene ~20 nm-thick HTL was generated with the same spin-coating and baking conditions as in HIL. For the realization of bicolored QD EL, two types of QD EML configurations of mixed QD EML *versus* bilayered QD EMLs were attempted. The former configuration was formed simply by blending CdZnS/ZnS and CIS/ZnS QD-hexane dispersions with the respective QD concentrations of ~30 and ~5 mg/ml. With the volume of CdZnS/ZnS QD dispersion fixed to be 1 ml, three blended QD solutions with different volumes of CIS/ZnS QD dispersion of 0.2, 0.5, and 0.8 ml, corresponding to CdZnS/ZnS-to-CIS/ZnS QD concentration weight ratios of 30, 12, and 7.5, respectively, were used for spin-deposition (3000 rpm, 20 s) of mixed QD EML. In the case of bilayered QD EMLs, a hexane dispersion of CIS/ZnS QDs with an identical QD concentration (~5 mg/ml) was spin-coated (2000 rpm, 20 s) on the underlying PVK layer. Prior to the direct spin-deposition of the second CdZnS/ZnS QD EML onto the preformed CIS/ZnS QD layer, which would damage the preformed CIS/ZnS QD layer, CIS/ZnS QD layer was surface-modified with a hydrophilic ligand of 3-mercaptopropionic acid (MPA) by spin-casting (1500 rpm, 60 s) an MPA-methanol solution with a volume ratio of 1:9, rinsing with methanol, and baking at 150^{o}C for 30 min in air. Then, the second EML was deposited by spin-casting (2000 rpm, 20 s) CdZnS/ZnS QD dispersion (QD concentration of ~20 mg/ml), forming bilayered QD EMLs with CIS/ZnS // CdZnS/ZnS QD (referred to as device B1). In such bilayer sequence, the thickness of CdZnS/ZnS QD layer was also varied by using the QD dispersion with different concentrations from the standard one (~20 mg/ml), with the thickness of CIS/ZnS QD layer unchanged. As a supplementary experiment, another bilayered QD EMLs with a reverse sequence of CdZnS/ZnS // CIS/ZnS QD and an identical intermediate MPA surface treatment were generated for a comparison. After the formation of either mixed QD EML or bilayered QD EMLs, ~32 nm-thick ETL of ZnO NPs was spin-deposited (1500 rpm, 60 s) using an ethanol dispersion with a concentration of ~30 mg/ml and baked at 60^{o}C for 30 min. The QLED fabrication was finalized by thermally evaporating a 100 nm-thick Al cathode on top of ETL. The device structure of multilayered QLED consisting of either mixed QD EML or bilayered QD EMLs was schematically illustrated in Fig. 1.

2.3 Characterization

Absorption and PL spectra of CdZnS/ZnS and CIS/ZnS QDs were measured by UV–visible absorption spectroscopy (Shimadzu, UV-2450) and a 500 W xenon lamp-equipped spectrophotometer (PSI Inc., Darsa Pro-5200), respectively. PL quantum yields (QYs) of QDs were assessed by an absolute PL QY measurement system (C9920-02, Hamamatsu) in an integrating sphere. Transmission electron microscopic (TEM) measurement was performed using a Tecnai G2 F20 operating at 200 kV to obtain particle images of QDs and cross-sectional image of a multilayered QLED. Various EL data such as EL spectrum, correlated color temperature (CCT), the Commission Internationale de l'Eclairage (CIE) color coordinates and CRI and luminance–current density–voltage characteristics of

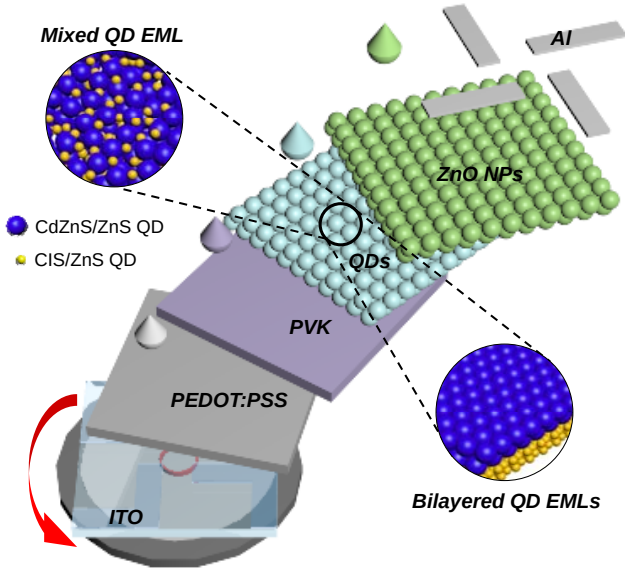

Fig. 1 Overall fabrication procedure of multilayered QLEDs consisting of either mixed QD EML or bilayered QD EMLs using a combination of blue CdZnS/ZnS and yellow CIS/ZnS QDs.

QLEDs were obtained with a Konica-Minolta CS-2000 spectroradiometer coupled with a Keithley 2400 voltage and current source under ambient conditions.

3 Results and discussion

Owing to the different pathways in radiative transition between CdZnS and CIS QDs, *i.e.*, excitonic *versus* intra-gap defect-involving recombination, respectively, the latter QDs possess a large Stokes-shift in emission *versus* absorption along with a substantially broadened bandwidth compared to the former ones, as seen in absorption (Fig. 2a) and normalized PL spectra (Fig. 2b). The blue (455 nm) CdZnS/ZnS and yellow (579 nm) CIS/ZnS QDs exhibited the emission bandwidths of 21 and 115 nm and QYs of 71 and 85%, respectively. As compared in TEM images (Fig. S1), a large size difference between such dissimilar QDs exists, showing the average diameters of 11.0 and 3.6 nm for blue and yellow QDs, respectively. Two monochromatic QLEDs, processed identically as depicted in Fig. 1 but comprising either blue CdZnS/ZnS or CIS/ZnS QD EML, were fabricated. Fig. 3a and b show voltage-dependent EL evolutions of blue and yellow QLEDs, respectively. The peak values of 3323 cd/m^2 (at 8 V) in luminance and 2.3 cd/A (at 6.5 V) in CE from the present blue (455 nm) QLED (Fig. S2a) were comparable to those from our earlier blue (452 nm) device.[6] Meanwhile, yellow QLED exhibited a peak luminance of 1707 cd/m^2 (at 7.5 V) and peak CE of 3.3 cd/A (at 6 V), whose values were also consistent with those reported very recently from our CIS/ZnS QD-based device.[14]

An initial attempt for achieving a bichromatic white QLED was to form a mixed QD EML by spin-casting the blended solutions of CdZnS/ZnS and CIS/ZnS QDs with appropriate QD ratios. Three blended QD solutions with different CdZnS/ZnS-to-CIS/ZnS QD weight ratios of 30, 12, and 7.5 were tested for device fabrication (referred to as device M1, M2, and M3, respectively, hereinafter). As shown in EL spectral variation as a function of applied voltage (Fig. 4a) of device M1, blue EL was prevailing with yellow EL barely observed (inset), indicating that the radiative recombination of charges injected from the electrodes occurred exclusively in blue QDs. In such mixed QD EML-based QLEDs, a simple increase in

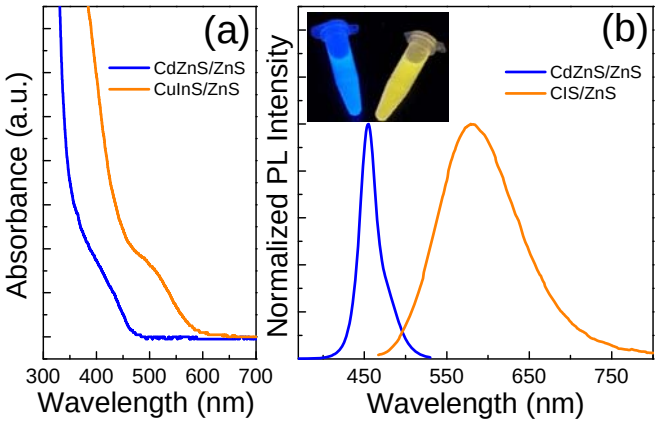

Fig. 2 (a) UV-visible absorption and (b) normalized PL spectra and fluorescent image (inset) of CdZnS/ZnS and CIS/ZnS QDs.

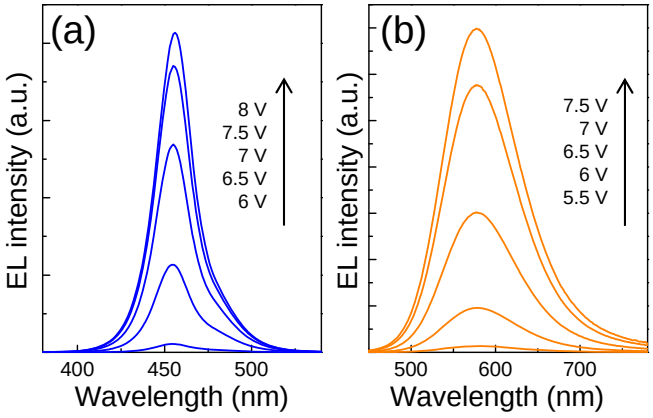

Fig. 3 EL spectral evolutions of (a) blue CdZnS/ZnS and (b) yellow CIS/ZnS monochromatic QLEDs with increasing applied voltage.

the content of CIS/ZnS QDs did not promote yellow EL effectively, as shown in Fig. 4b and c for device M2 and M3, respectively, although it led to a slight increment of CIS/ZnS QD EL. The areal contribution of yellow components in overall EL spectra reached only 11–18% for device M3, depending on applied bias. Förster resonant energy transfer (FRET) from CIS/ZnS QDs to neighboring CdZnS/ZnS ones would not be responsible for such significant EL quenching of CIS/ZnS QDs, taking into account that the spectral overlap between the emission of smaller band gap-yellow QDs and the absorption of larger band gap-blue ones is naturally absent (Fig. 2). As noticed from the above QD blending ratios, it is naturally expected that in the mixed QD EML a major constituent would be large-sized CdZnS/ZnS QDs with small-sized CIS/ZnS ones embedded between them. Therefore, the electrical contacts of the mixed QD EML with adjacent charge transport layers would originate mainly from CdZnS/ZnS QDs, leading to the dominant excitonic recombination in blue QDs. To elicit a more noticeable yellow EL a blended solution having a CdZnS/ZnS-to-CIS/ZnS QD weight ratios much smaller than 7.5 (*e.g.*, 2) was applied for device fabrication, however, its performance was severely deteriorated, probably attributable to the inhomogeneous EML formation resulting from the inappropriate blending ratio between large-sized CdZnS/ZnS QDs and small-sized CIS/ZnS ones.

To realize the desired bicolored white EL, CIS/ZnS and CdZnS/ZnS QDs were sequentially deposited in the bilayer form of CIS/ZnS // CdZnS/ZnS QD (Fig. 1). To prevent an interlayer mixing

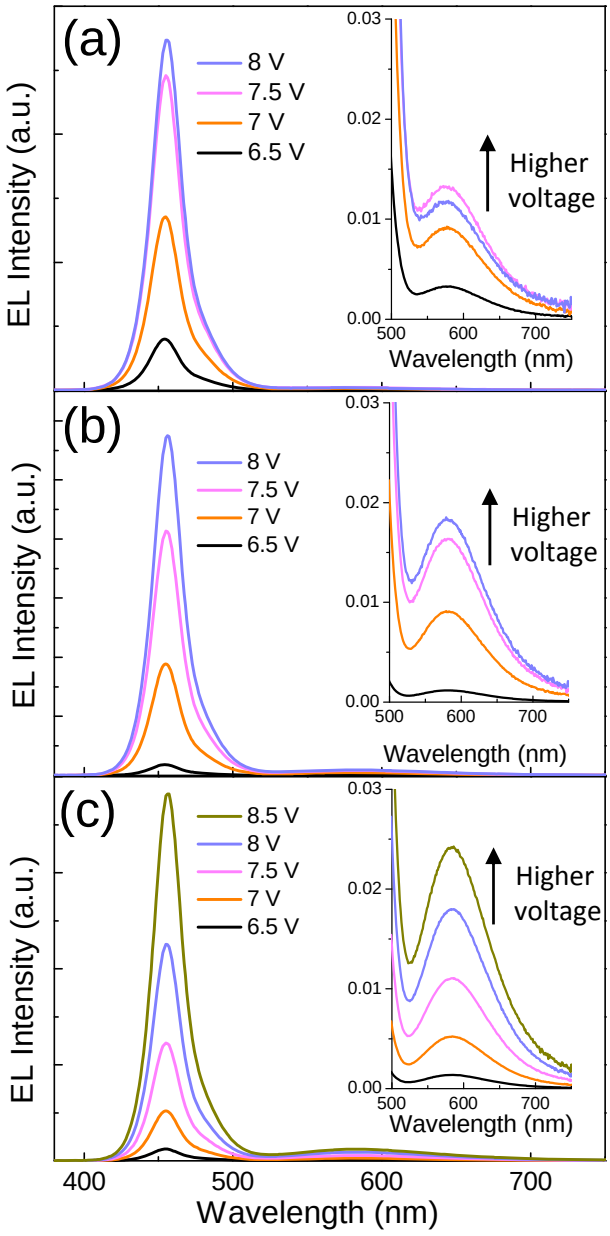

Fig. 4 Voltage-dependent EL spectral evolutions of the QLEDs comprising the EML of mixed QDs with CdZnS/ZnS-to-CIS/ZnS QD weight ratios of (a) 30, (b) 12, and (c) 7.5. The respective insets present the magnified spectral regions of CIS/ZnS QD EL.

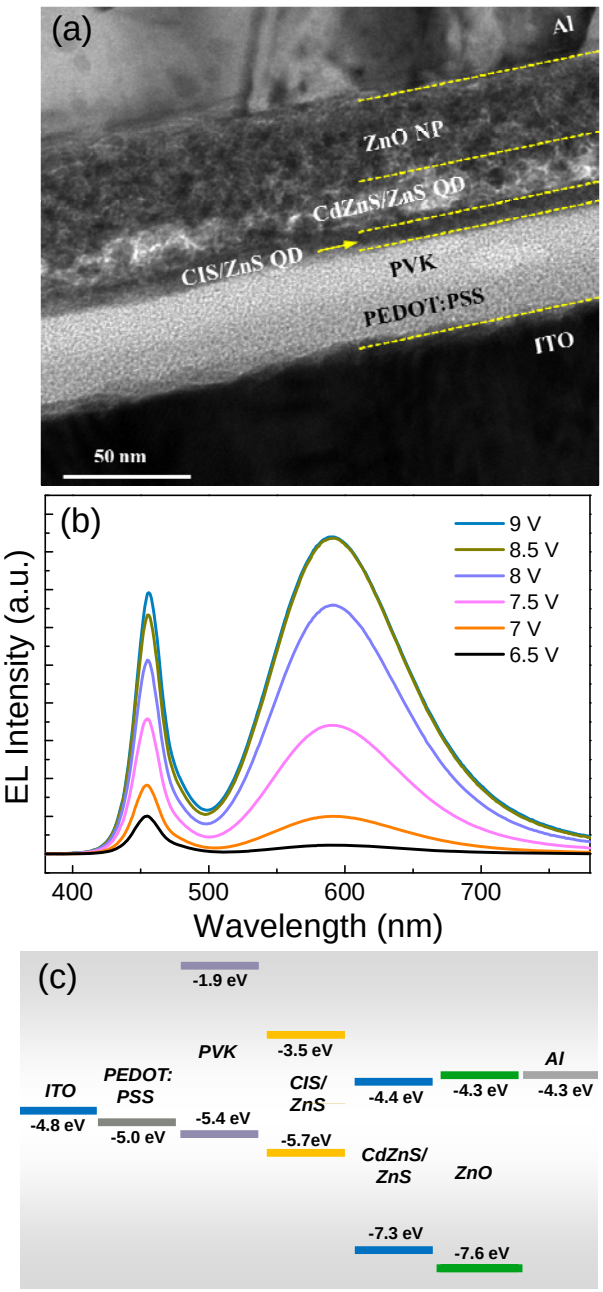

Fig. 5 (a) Cross-sectional TEM micrograph, (b) voltage-dependent EL spectral evolution, and (c) proposed energy band diagram of bilayered QD EML-based QLED with a stacking sequence of CIS/ZnS // CdZnS/ZnS QD (device B1).

that may occur when two QDs are consecutively spin-casted, the surface of preformed CIS/ZnS QD layer was treated with a hydrophilic MPA, and then the second layer of CdZnS/ZnS QDs was deposited. A cross-sectional TEM image of the fabricated QLED (device B1) comprising such a bilayer QD EML is shown in Fig. 5a, where the bilayer formation can be distinctly observed with the thicknesses of ~7 and ~21 nm for CIS/ZnS and CdZnS/ZnS QD layer, respectively. As shown in EL spectral evolution with increasing applied bias (Fig. 5b), bicolored white EL emissions were achievable as a consequence of successful charge recombination in both QD regions. These results are contrast to the previous work on II–VI QLEDs with different stacking sequences of two colored QD layers, where the recombination zone was mostly confined to the top QD monolayer adjacent to ETL.[25] According to the energetic information on CIS/ZnS,[26] CdZnS/ZnS QDs,[6,27,28] and ZnO NPs[1] in literature, the energy band diagram of multilayered white QLED was constructed (Fig. 5c). The energetic correlation between CdZnS *versus* CIS QD corresponds to a type II electronic band structure, specifically, the valence and conduction bands of CIS QD are all higher in energy than those of CdZnS counterpart. As can be inferred from EL results of Fig. 5b, a part of electrons injected to blue QD EML from cathode side would overcome the energy offset of 0.9 eV at CIS/ZnS // CdZnS/ZnS QD interface, radiatively recombining with an injected hole at CIS/ZnS QD. Meanwhile, a hole injected to CIS/ZnS QD experiences a relatively large energy barrier of 1.6 eV for a further injection to CdZnS/ZnS QD. In this situation where

holes and electrons are accumulated at CIS/ZnS and CdZnS/ZnS QD region, respectively, an Auger-assisted hole injection process from the former to latter QD layer is likely operative,[1,4] simultaneously leading to the radiative recombination of an injected hole with an electron on standby at CdZnS/ZnS QD. For comparison, another QLED with the reverse bilayer configuration of CdZnS/ZnS // CIS/ZnS QD was also fabricated. Note here that the intermediate MPA treatment was identically applied for interlayer mixing-free bilayer formation. Intriguingly, its EL spectra (Fig. S3a) were far from white emission, being rather similar to those of mixed QD EML-based devices (Fig. 4). Such an almost single blue EL may be also justified with the energy band diagram with the positions of two QD layers inter-switched (Fig. S3b). When compared to the energy offset (0.8 eV) for electron injection from ZnO NP ETL to CIS/ZnS QD, a larger offset (1.9 eV) for hole injection from PVK to CdZnS/ZnS QD is established, by which the carrier injection becomes dominated by the electron. The electrons passing through CIS/ZnS QD layer arrive at and become accumulated in CdZnS/ZnS QD layer prior to a direct hole injection to CdZnS/ZnS QD from PVK. At this point, an Auger-assisted hole injection mechanism aforementioned would be identically valid. Most of such Auger-injected holes would participate in the radiative recombination with the electrons sufficiently accumulated at CdZnS/ZnS QD region, by which the chance for electrons to reach CIS/ZnS QD layer becomes rarified.

In the QD bilayer configuration of CIS/ZnS // CdZnS/ZnS, the spectral ratio of blue-to-yellow (B/Y) EL has been tuned by varying the thickness of blue QD layer with that of yellow QD one fixed. Simply using blue QD dispersions having the lower (*i.e.*, ~16 mg/ml) *versus* higher concentrations (*i.e.*, ~28 mg/ml) than that (*i.e.*, ~20 mg/ml) adopted for the above device B1, another two QLEDs, hereinafter denoted as device B2 and B3, respectively, were fabricated. Device B2 exhibited substantially reduced B/Y EL ratios (Fig. 6a), as compared with those from device B1 (Fig. 5b). The opposite trend in the spectral distribution can be also observed when a thicker blue QD layer (device B3) was applied (Fig. 6b). Such spectral modulation with varying blue QD layer thickness is likely associated with the leakage electron flow. The leakage electrons passing across blue QD layer would depend on its thickness, specifically increasing with decreasing thickness. Hence, as compared with device B3, the number of electron reaching yellow QD layer should be more for device B2, providing a higher possibility of charge recombination at CIS/ZnS relative to CdZnS/ZnS QD region. In addition, the incomplete QD coverage on top of the yellow QD layer upon decreasing the thickness of blue QD layer (device B2), presumably causing the direct contact of CIS/ZnS QD with ZnO NP ETL through the vacant sites in the top CdZnS/ZnS QD layer, may be partly responsible for the dominant yellow EL. To examine the B/Y spectral evolution as a function of applied voltage, the respective EL spectra of device B2 and B3 were normalized to the yellow EL (Fig. S4). Device B2 exhibited a slightly increasing tendency in B/Y ratio (Fig. S4a), that is, a relatively decreasing contribution of yellow EL *versus* blue EL at a higher voltage. This may be rationalized by the charging of CIS/ZnS QDs, where most of carrier recombination occurs. The exciton in charged QDs loses its energy nonradiatively *via* an efficient Auger decay,[6,29,30] and thus a gradually decreasing contribution of yellow EL in Fig. S4a is attributable to a more intense degree of CIS/ZnS QD charging under a higher current density. In the case of device B3, the B/Y spectral dependence on voltage was in an opposite fashion compared to device B2, showing a marked reduction of B/Y ratio with increasing bias (Fig. S4b). This can be also explained by the above QD charging effect, but such a charging would become dominant in CdZnS/ZnS QDs over CIS/ZnS ones for device B3,

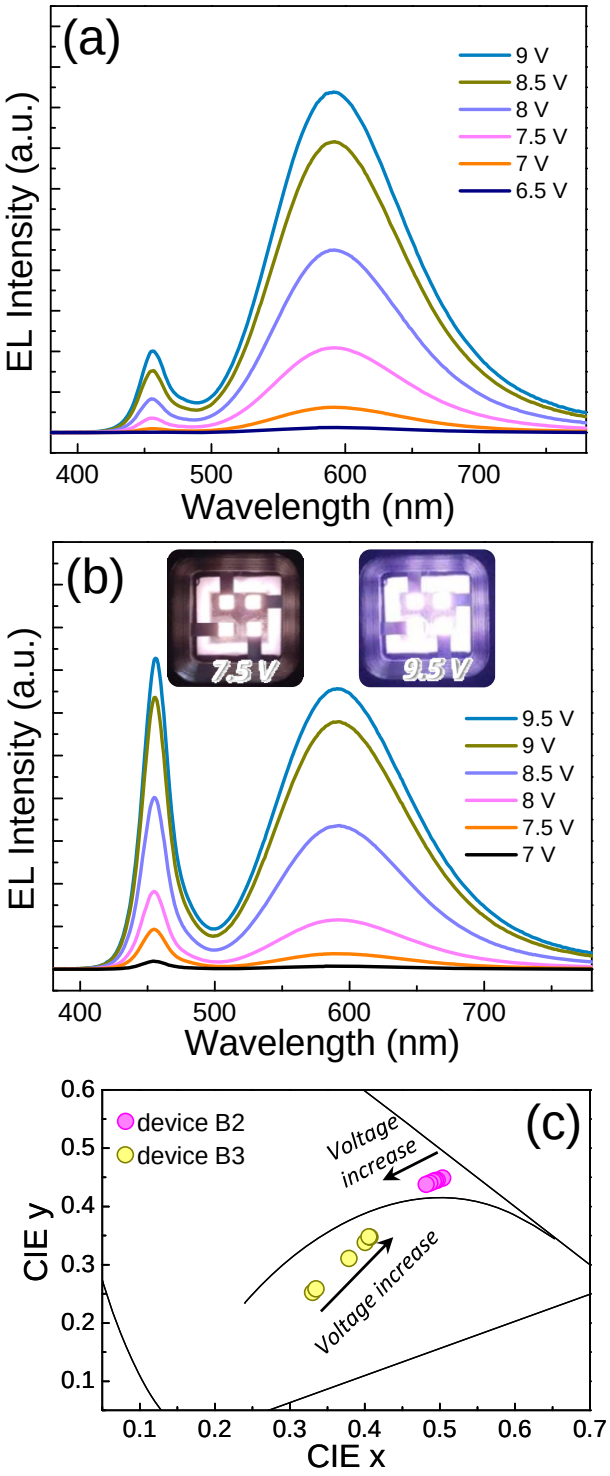

Fig. 6 Voltage-dependent bicolored EL evolutions of CIS/ZnS // CdZnS/ZnS QD-bilayered QLEDs with (a) thin (device B2) and (b) thick CdZnS/ZnS QD layer (device B3), with the thickness of CIS/ZnS QD underlayer unchanged. (c) Variations of CIE color coordinates of white EL of device B2 and B3 with increasing voltage.

since the presence of a thick blue QD layer limits the supply of electrons to yellow QD layer, rendering the charging of yellow QD more relaxed. These voltage-dependent B/Y spectral variations for device B2 and B3 are reflected in CIE color coordinates (Fig. 6c), where the color shifts with voltage increase were in an opposite

direction for the respective devices, *e.g.*, (0.504, 0.449) at 6.5 V → (0.482, 0.438) at 9 V for device B2 and (0.330, 0.253) at 7 V → (0.405, 0.348) at 9.5 V for device B3. As expected from the spectral shapes (Fig. 6a and b), device B2 and B3 exhibited warmer and cooler white emissions having CCTs of 2465–2637 K and 3084–5494 K, respectively, depending on applied bias. While moderate CRIs of 63–67 were obtainable from device B2, device B3 showed relatively low values of 45–52. Such limited color rendering property is primarily ascribed to the spectral deficiency in cyan-green region.

The variations of luminance and current density with a voltage sweep to 11 V for two QLEDs with thin (device B2) and thick blue QD layer (device B3) are compared in Fig. 7a. As a natural consequence of increased QD layer the current densities of device B3 were lower than those of device B2 particularly at high voltage biases. Luminances were higher for device B2 *versus* device B3 throughout the entire voltage, specifically displaying the peak values of 786 (at 9 V) and 678 cd/m^2 (at 9.5 V) respectively, mainly attributable to higher current flow from the former than the latter device. Compared to device B3 overall efficiencies of device B2 were higher, showing double peak values (Fig. 7b). The peak values of device B2 and device B3 were 1.4 and 0.7 cd/A in CE, 0.6 and 0.3 lm/W in power efficiency (PE), and 0.6 and 0.3% in EQE, respectively. The above peak efficiency values of both devices were identically obtained at an applied bias of 7 V, where the luminances of 56 and 21 cd/m^2 were recorded for device B2 and B3, respectively. Device performances of those bilayer QLEDs were inferior with

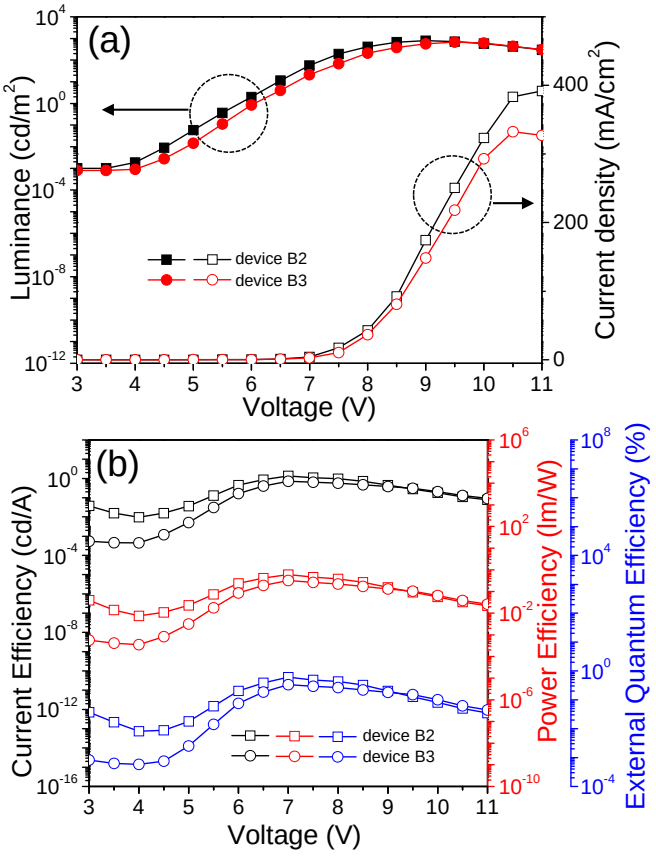

Fig. 7 Variations of (a) luminance–current density and (b) CE–PE–EQE as a function of applied voltage of bilayered EML-based QLEDs of device B2 and B3.

respect to both luminance and efficiencies as compared to those of the monochromatic (blue and yellow) devices aforementioned. One plausible reason is likely associated with a substantially limited current flow in bilayer QLEDs relative to monochromatic devices (Fig. S5a), resulting from not only the increased EML thickness but the MPA treatment introduced at the interface of CIS/ZnS // CdZnS/ZnS QD layers. The presence of interfacial MPA layer is necessary for the formation of interlayer-mixing free QD bilayer, but would rather limit a smooth current flow by its insulating attribute. Moreover, an MPA baking temperature of 150^{o}C optimized experimentally for anchoring the hydrophilic ligand onto the surface of the first CIS/ZnS QD layer appears to be too high when compared to the conventional QD EML baking temperatures (<100^{o}C), probably deteriorating EL performance. Such a detrimental effect of high baking temperature was verified by evaluating a CIS/ZnS QLED additionally fabricated with the identical processing conditions except for EML baking temperature, *i.e.*, 150^{o}C instead of 60^{o}C. The resulting QLED possessed appreciably lowered EL values, as compared to the control device (60^{o}C baking) (Fig. S2b), only reaching the peak values of 1170 cd/m^2 in luminance and 0.9 cd/A in CE (Fig. S5b).

4 Conclusions

For an effort to demonstrate a white EL through a QD combination of blue CdZnS/ZnS and yellow CIS/ZnS QD emitters, different QD EML configurations in the fabrication of multilayered hybrid QLED were attempted, finding that the inter-QD positioning in device architecture plays a critical role in obtaining a bicolored white emission. The QLED comprising either mixed QD EML or CdZnS/ZnS // CIS/ZnS QD bilayered EML was not capable of generating a satisfactory white emission, resulting in an unequally high B/Y spectral ratio. On the other hand, the device fabricated with another bilayer sequence of CIS/ZnS // CdZnS/ZnS QD successfully exhibited a bicolored white EL owing to the extended excitonic recombination zone throughout both QD EML regions. The B/Y EL spectral ratio was controllable by varying the thickness of CdZnS/ZnS QD overlayer with the thickness of CIS/ZnS QD underlayer fixed, being observed to be higher with increasing overlayer thickness. Depending on the overlayer thickness and applied bias, these white QLEDs possessed CCTs of 2465–5494 K, CRIs of 45–67, and peak values of 678–786 cd/m^2 in luminance, 0.7–1.4 cd/A in CE, 0.3–0.6 lm/W in PE, and 0.3–0.6 % in EQE.

Acknowledgements

This work was supported by the National Research Foundation of Korea (NRF) grant funded by the Korea government (MSIP) (No. 2013R1A2A2A01068158).

Notes and references

[a] Department of Materials Science and Engineering, Hongik University, Seoul 121-791, Korea
Email address: hyang@hongik.ac.kr
[b] Institute of Advanced Composite Materials, Korea Institute of Science and Technology, Jeonbuk 565-905, Republic of Korea
[c] Center for Materials Architecturing, Korea Institute of Science and Technology, Seoul 136-791, Korea
[d] Department of Chemistry, Kookmin University, Seoul 136-702, Korea

† Electronic Supplementary Information (ESI) available: Detailed description of synthesis of CdZnS/ZnS, CIS/ZnS QDs, and ZnO NPs, TEM images of CdZnS/ZnS and CIS/ZnS QDs, voltage-dependent luminance–CE variations of blue CdZnS/ZnS and yellow CIS/ZnS monochromatic QLEDs, EL spectra and energy band diagram of bilayered QD EML-based QLED with a stacking sequence of CdZnS/ZnS // CIS/ZnS QD, normalized EL spectra of CIS/ZnS // CdZnS/ZnS QD-bilayered QLEDs, comparison of current density of monochromatic

QLEDs and bicolored white QLEDs, and voltage-dependent luminance–CE variations of CIS/ZnS QLED fabricated through 150°C-EML baking.. See DOI: 10.1039/b000000x/

1 L. Qian, Y. Zheng, J. Xu and P. H. Holloway, *Nat. Photonics*, 2011, **5**, 543–548.
2 J. Kwak, W. K. Bae, D. Lee, I. Park, J. Lim, M. Park, H. Cho, H. Woo, Y. Yoon, K. Char, S. Lee and C. Lee, *Nano Lett.*, 2012, **12**, 2362–2366.
3 Y. Shirasaki, G. J. Supran, M. G. Bawendi and V. Bulovic, *Nat. Photonics*, 2013, **7**, 13–23.
4 B. S. Mashford, M. Stevenson, Z. Popovic, C. Hamilton, Z. Q. Zhou, C. Breen, J. Steckel, V. Bulovic, M. Bawendi, S. Coe-Sullivan and P. T. Kazlas, *Nat. Photonics*, 2013, **7**, 407–412.
5 X. Dai, Z. Zhang, Y. Jin, Y. Niu, H. Cao, X. Liang, L. Chen, J. Wang and X. Peng, *Nature*, 2014, **515**, 96–99.
6 K. H. Lee, J. H. Lee, W. S. Song, H. Ko, C. Lee, J. H. Lee and H. Yang, *ACS Nano*, 2013, **7**, 7295–7302.
7 K. H. Lee, J. H. Lee, H. D. Kang, B. Park, Y. Kwon, H. Ko, C. Lee, J. Lee and H. Yang, *ACS Nano*, 2014, **8**, 4893–4901.
8 J. Lim, W. K. Bae, D. Lee, M. K. Nam, J. Jung, C. Lee, K. Char and S. Lee, *Chem. Mater.*, 2011, **23**, 4459–4463.
9 X. Yang, D. Zhao, K. S. Leck, S. T. Tan, Y. X. Tang, J. Zhao, H. V. Demir and X. W. Sun, *Adv. Mater.*, 2012, **24**, 4180–4185.
10 X. Y. Yang, Y. Divayana, D. W. Zhao, K. S. Leck, F. Lu, S. T. Tan, A. P. Abiyasa, Y. B. Zhao, H. V. Demir and X. W. Sun, *Appl. Phys. Lett.*, 2012, **101**, 233110.
11 Z. Tan, Y. Zhang, C. Xie, H. Su, J. Liu, C. Zhang, N. Dellas, S. E. Mohney, Y. Wang, J. Wang and J. Xu, *Adv. Mater.*, 2011, **23**, 3553–3558.
12 B. K. Chen, H. Z. Zhong, W. Q. Zhang, Z. A. Tan, Y. F. Li, C. R. Yu, T. Y. Zhai, Y. S. Bando, S. Y. Yang and B. S. Zou, *Adv. Funct. Mater.*, 2012, **22**, 2081–2088.
13 J. Lim, M. Park, W. K. Bae, D. Lee, S. Lee, C. Lee and K. Char, *ACS Nano*, 2013, **7**, 9019–9026.
14 J. H. Kim, K. H. Lee, D. Y. Jo, Y. Lee, J. Y. Hwang and H. Yang, *Appl. Phys. Lett.*, 2014, **105**, 133104.
15 T. H. Kim, K. S. Cho, E. K. Lee, S. J. Lee, J. Chae, J. W. Kim, D. H. Kim, J. Y. Kwon, G. Amaratunga, S. Y. Lee, B. L. Choi, Y. Kuk, J. M. Kim and K. Kim, *Nat. Photonics*, 2011, **5**, 176–182.
16 P. O. Anikeeva, J. E. Halpert, M. G. Bawendi and V. Bulovic, *Nano Lett.*, 2007, **7**, 2196–2200.
17 W. K. Bae, J. Lim, D. Lee, M. Park, H. Lee, J. Kwak, K. Char, C. Lee and S. Lee, *Adv. Mater.*, 2014, **26**, 6387–6393.
18 L. Li, A. Pandey, D. J. Werder, B. P. Khanal, J. M. Pietryga and V. I. Klimov, *J. Am. Chem. Soc.*, 2011, **133**, 1176–1179.
19 W. S. Song and H. Yang, *Chem. Mater.*, 2012, **24**, 1961–1967.
20 B. Chen, H. Zhong, M. Wang, R. Liu and B. Zou, *Nanoscale*, 2013, **5**, 3514–3519.
21 P. H. Chuang, C. C. Lin and R. S. Liu, *ACS Appl. Mater. Interfaces*, 2014, **6**, 15379–15387.
22 K. Lim, H. S. Jang and K. Woo, *Nanotechnology*, 2012, **23**, 485609.
23 K. H. Lee, J. H. Lee, H. D. Kang, C. Y. Han, S. M. Bae, Y. Lee, J. Y. Hwang and H. Yang, *J. Alloy Compd.*, 2014, **610**, 511–516.
24 J. H. Kim and H. Yang, *Opt. Lett.*, 2014, **39**, 5002–5005.
25 W. K. Bae, J. Kwak, J. Lim, D. Lee, M. K. Nam, K. Char, C. Lee and S. Lee, *Nano Lett.*, 2010, **10**, 2368–2373.
26 X. Yuan, J. L. Zhao, P. T. Jing, W. J. Zhang, H. B. Li, L. G. Zhang, X. H. Zhong and Y. Masumoto, *J. Phys. Chem. C*, 2012, **116**, 11973–11979.
27 W. K. Bae, J. Kwak, J. Lim, D. Lee, M. K. Nam, K. Char, C. Lee and S. Lee, *Nanotechnology*, 2009, **20**, 075202.
28 H. B. Shen, X. W. Bai, A. Wang, H. Z. Wang, L. Qian, Y. X. Yang, A. Titov, J. Hyvonen, Y. Zheng and L. S. Li, *Adv. Funct. Mater.*, 2014, **24**, 2367–2373.
29 W. K. Bae, Y. S. Park, J. Lim, D. Lee, L. A. Padilha, H. McDaniel, I. Robel, C. Lee, J. M. Pietryga and V. I. Klimov, *Nat. Commun.*, 2013, **4**, 2661.
30 J. Lim, B. Jeong, M. Park, J. K. Kim, J. M. Pietryga, Y.-S. Park, V. I. Klimov, C. Lee, D. C. Lee and W. K. Bae, *Adv. Mater.*, 2014, **26**, 8034–8040.